Monte Carlo simulation of DNA damage induction by x-rays and selected radioisotopes

Y Hsiao[1] **and R D Stewart**[2]

[1] Department of Physics, Purdue University, West Lafayette, IN 47907-2036, USA
[2] School of Health Sciences, Purdue University, West Lafayette, IN 47907-2051, USA

E-mail: trebor@purdue.edu

Abstract

To better assess the potential biological consequences of diagnostic x-rays and selected γ-emitting radioisotopes used in brachytherapy, we used the PENELOPE Monte Carlo radiation transport code to estimate the spectrum of initial electrons produced by photons in single cells and in an irradiation geometry similar to those used in cell culture experiments. We then combined estimates of the initial spectrum of electrons from PENELOPE with DNA damage yields for monoenergetic electrons from the fast Monte Carlo damage simulation (MCDS). The predicted absolute yields (Gbp^{-1} Gy^{-1}) and RBE values for single-strand break (SSB) and double-strand break (DSB) induction by 220 kVp x-rays are within 1% of the results from detailed track-structure simulations (Friedland *et al* 1999 *Radiat. Environ. Biophys.* **38** 39). The measured RBE for DSB induction reported by Kühne *et al* (2005 *Radiat. Res.* **164** 669) for γ-rays from ^{60}Co and for 29 kVp x-rays with a 50 μm Rh (mammography) filter are in excellent agreement (1.15 versus 1.16). DSB yields predicted by the MCDS also agree to within 7% with the absolute DSB yields reported by de Lara *et al* (2001 *Radiat. Res.* **155** 440) and Botchway *et al* (1997 *Radiat. Res.* **148** 317) for the irradiation of V79 cells by low energy (<2 keV) characteristic x-rays. The predicted RBE for DSB induction by γ-rays from bare ^{169}Yb and ^{131}Cs to ^{60}Co are 1.06 and 1.14, respectively. Tabulated RBE values for the single-cell and monolayer cell culture geometries differ by at most 15%. The proposed methodology is computationally efficient and may also be useful for the prediction of damage yields for mixtures of other types of charged particles, such as those found in proton therapy, space applications or internal dosimetry.

1. Introduction

Low-energy photons are frequently used in laboratory experiments and clinical procedures, including brachytherapy and mammography. Although photons are nearly always considered a low linear energy transfer (LET) radiation, experiments have demonstrated that not all photons have the same relative biological effectives (RBE) for double-strand break (DSB) induction (de Lara *et al* 2001, Kühne *et al* 2005, Claesson *et al* 2007) and clonogenic survival (Spadinger and Palcic 1992, Plume *et al* 1993, Ling *et al* 1995, Frankenberg *et al* 2002). In general, the RBE for cell survival increases with increasing LET up to about 100 keV μm^{-1} (Hall 2000). Studies have also shown that the RBE for double-strand break (DSB) induction increases with increasing LET up to at least 10–40 keV μm^{-1} (Frankenberg *et al* 1999, Belli *et al* 2000, de Lara *et al* 2001), which is consistent with the hypothesis that DSB are one of the more lethal forms of DNA damage induced by ionizing radiation (Ward 1988, Goodhead 1994, Kundrát and Stewart 2006).

The passage of x-rays and γ-rays through a cell produces a cascade of secondary electrons through photoelectric and other interaction mechanisms, and the effective LET of this cascade of secondary electrons tends to increase as the energy of the primary photon decreases. These observations imply that the radioisotopes emitting lower energy photons, such as ^{131}Cs and ^{125}I, are potentially more biologically effective, per unit-absorbed dose, than photons from radioisotopes such as ^{137}Cs or ^{60}Co. Although several studies have reported RBE values for cell survival after irradiation by ^{125}I, ^{169}Yb and ^{192}Ir sources (Hering 1980, Freeman *et al* 1982, Marchese *et al* 1984, Plume *et al* 1993, Ling *et al* 1995, Lehnert *et al* 2005), we are not aware of any published study reporting information on the RBE of ^{169}Yb and ^{192}Ir for DSB induction. Also, the radioisotope ^{131}Cs is a new photon-emitting brachytherapy source (Rivard (2007) and references therein), and no information on the RBE of this isotope is currently available in the literature. Information on the RBE of lower energy γ-ray emitting radioisotopes and x-ray sources is needed to better predict the efficacy of brachytherapy and to better assess the risks of diagnostic procedures.

The fast Monte Carlo damage simulation (MCDS) proposed by Semenenko and Stewart (2004, 2006) provides nucleotide-level maps of clustered DNA lesions, including single-strand breaks (SSBs) and double-strand breaks (DSBs), that are comparable to the damage yields obtained from computationally expensive, but more detailed, track structure simulations. Although able to simulate the induction of clustered damage produced electrons, protons and α particles with energies as high as $\sim$1 GeV, the MCDS has no capabilities for the direct determination of damage yields for photons (or other neutral particles). In this paper, we develop a methodology to estimate the yields of clustered DNA lesions from the distribution of secondary electrons produced through the absorption or scattering of the photons incident on single cells and cells in monolayer cell cultures. The latter study was conducted to assess the potential impact on RBE values of attenuation and scattering of the primary radiation beam in a geometry that more closely mimics those used in laboratory experiments. To validate the proposed methodology, estimates of damage yields and RBE values for selected radioisotopes and x-ray spectra are compared to estimates from the literature. The reported studies provide new information to better assess the biological effectiveness of diagnostic x-rays and selected low-energy γ-ray emitting isotopes used in brachytherapy applications.

2. Material and methods

The MCDS (Semenenko and Stewart 2004, 2006) provides estimates of the yield of clustered damage after *uniform irradiation* of a cell (i.e. the absorbed dose is constant everywhere within

the cell) by monoenergetic electrons, protons or α particles. Because MCDS damage yields implicitly account for clusters caused by the cascade of secondary electrons produced by the passage of a primary charged particle through or near a cell, damage yields for a mixture of charged particles can be determined by weighting the MCDS yields by the fluence of primary charged particles. The primary charged particles of interest for photons with energies less than about 10 MeV are the initial electrons produced through photoelectric absorption, Compton scattering and pair production interactions. Electrons with kinetic energies less than 10 MeV, the peak energy possible for a 10 MeV photon, have an unrestricted LET greater than 0.2 keV μm^{-1}. Because the number of ionizations produced in cellular targets by secondary electrons far exceeds the number of ionization events produced through primary photon interactions, secondary electrons most likely play a decisive role in causing DNA damage. This hypothesis is supported by the observation that the biological effects induced by photons are comparable to the biological effects induced by the secondary electrons alone (Nikjoo and Goodhead 1991, Ottolenghi *et al* 1997, Walicka *et al* 1998, Kellerer 2002).

The above observations suggest that the induction of clustered damage by low-energy photons can be computed using a two-step methodology. First, estimate the initial spectrum of secondary electrons produced in a biological target through the interactions of incident (unscattered) and scattered photons. These secondary electrons can now be considered the 'primary charged particle' and used to compute spectrum-averaged cluster yields from the damage yields for monoenergetic electrons estimated with the MCDS. Additional details of the methodology used to compute spectrum-averaged damage yields in single-cell and monolayer cell culture geometry are outlined below.

2.1. Irradiation geometries and materials

The two geometries used to simulate the induction of damage in a representative mammalian cell are shown in figure 1. The single-cell geometry follows the geometry used by Friedland *et al* (1999). Cells are modeled as a cylinder shape with a diameter of 20 μm and a height of 20 μm. The single-cell irradiation geometry also includes a 4 μm mylar foil (density 1.4 g cm^{-3}) between the photon beam and the cell. Because low-energy photons and charged particles may be substantially attenuated by even small thicknesses of water or plastic, we also set up a monolayer cell culture geometry to better mimic the irradiation geometry used in typical laboratory experiments. To model a layer of cells attached to the bottom of a culture dish, we used a cylinder with a diameter of 52 mm and a height of 5 mm. For both irradiation geometries, cells and the culture medium were approximated by water at a density of 1.0 g cm^{-3}. To estimate the particle fluence in a layer of cells attached to the bottom of the culture dish, we tallied the particle fluence in two parallel planes separated by 10 μm, as illustrated in figure 1. For simulations with γ-emitting radioisotopes (^{60}Co, ^{137}Cs, ^{192}Ir, ^{169}Yb, ^{131}Cs, ^{125}I), the photon source was modeled with and without a 50 μm titanium shell to investigate possible differences in damage yields for bare and encapsulated brachytherapy seeds (e.g., as in Chen *et al* (2005)).

2.2. Determination of secondary electron fluence with PENELOPE

We used the PENCYL computer program distributed with the PENELOPE Monte Carlo radiation transport software package (Baró *et al* 1995, Sempau *et al* 1997, Salvat *et al* 2003, 2005) to determine the fluence of electrons traversing single cells and cells in monolayer cell cultures (refer to figure 1). All simulations were performed using the 2005 version of PENELOPE (Salvat *et al* 2005), which is able to transport electrons and positrons with
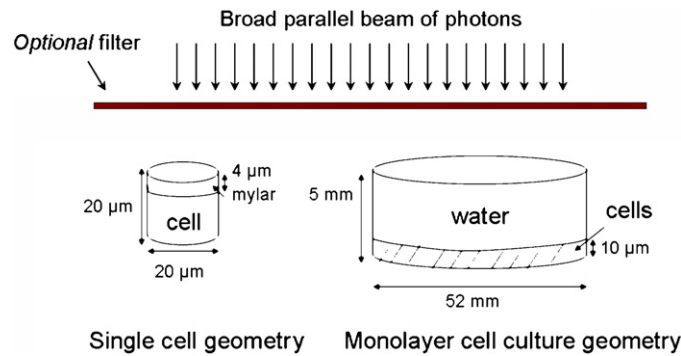
Figure 1. Irradiation geometries used to simulate damage yields in single cells (left) and monolayer cell cultures (right). Particle fluences are tallied in planes perpendicular to the incident photon beam above and below the location of the cell and monolayer cell culture.

kinetic energies as low as 50 eV. PENELOPE uses a scattering model (Baró *et al* 1995) that combines analytical cross-section models for different interaction mechanisms with numerical databases (Salvat *et al* 2005). The cross-section tables for different photon and electron interactions as well as temporary storage of secondary particles created during the transport of a primary (source) particle are automatically handled within the PENELOPE transport kernel. A complete PENELOPE application consists of the PENELOPE transport kernel and a set of user-supplied routines to record the location of energy transfer events, control the overall evolution of particle tracks and determine the geometry of the materials used in the simulation. PENELOPE has been shown to be useful to estimate microdosimetric quantities (Stewart *et al* 2002) and can be used to simulate complex arrangements of materials, such as those found in the human body or *in vitro* experiments.

Because the PENCYL program only provides tallies of the particle fluence across the planes dividing adjacent cylinders, we computed the energy fluence of photons and electrons just above and below the location of the cell (left panel, figure 1) or cell layer (right panel, figure 1). Comparisons of the electron and photon energy fluence for ^{125}I, which emits the lowest photon energies studied in this work, above and below the cell differ by less than 20%, which suggests that the particle fluence and absorbed dose is constant everywhere within the cell for the considered irradiation geometries. Consequently, the surface used to tally particle fluence will have a negligible impact on estimates of damage yields. All of the reported results are based on estimates of particle fluence tallied on planes located distal to the incident photon beam (refer to figure 1). We used the PENCYL default of 100 energy bins to tally particle fluences in all simulations.

All PENCYL simulations were performed with at least 2×10^8 source particle histories, which ensure that estimates of the secondary electron energy fluence are accurate to within about 6%. X-ray spectra were simulated by targeting a cylindrical tungsten target 0.2 mm thick with at least 5×10^7 electrons with kinetic energies of 29 keV, 130 keV and 220 keV. For the 29 keV x-ray simulations, x-ray spectra were generated with a 50 μm rhodium filter (Kühne *et al* 2005) and a 30 μm molybdenum filter (Verhaegen and Reniers 2004) to simulate other published geometries. The calculated 29 kVp x-ray spectrum with rhodium filter is typical of those used for mammography and is in excellent agreement with the spectra reported by Säbel and Aichinger (1996). The geometry used to simulate the 130 kVp x-ray spectra includes a 0.4 mm Cu filter, and the geometry used to determine the 220 kVp x-ray spectrum includes

0.5 mm Cu and 4 mm Al filters (Friedland *et al* 1999). Photon spectra (bare source) for the selected isotopes (^{60}Co, ^{137}Cs, ^{192}Ir, ^{169}Yb, ^{125}I and ^{131}Cs) were taken from the National Nuclear Data Center (NNDC) (Berger *et al* 2005).

PENELOPE combines a mixed electron and positron simulation with event-by-event simulation of major photon interactions. The mixed simulation algorithm (Baró *et al* 1995) permits the simulation of high-energy electron and positron transport more quickly. The level of detail included in the simulation of electron transport processes is controlled in PENELOPE by specifying values for several parameters, C_1, C_2, W_{CC} and W_{CR}, whose definitions and roles are explained in detail elsewhere (Salvat *et al* 2005). Briefly, C_1 controls average angular deflection produced by multiple elastic scattering of electrons along the step between hard events and C_2 controls the maximum average fractional energy loss in the step. W_{CC} and W_{CR}, respectively, represent the cutoff energy loss for hard inelastic collisions and for hard bremsstrahlung emission. With larger values of these parameters, the simulation executes faster at the expense of less accuracy in the simulation of radiation transport. To generate the 29 kVp, 130 kVp and 220 kVp x-ray spectra, we used $C_1 = 0.2$, $C_2 = 0.1$, $W_{CC} = 1$ keV, $W_{CR} = 1$ keV. For electron-emitting radioisotopes, the parameters were selected to give a detailed treatment of electron elastic and inelastic collisions ($C_1 = 0.00$, $C_2 = 0.01$). Electrons and positrons with kinetic energies below 100 eV and photons with energies less than 1 keV are assumed to deposit all their energy locally ($W_{CC} = 100$ eV, $W_{CR} = 100$ eV).

2.3. Spectrum-averaged DNA damage yields

Let $\Sigma_i(E)$ denote the initial yield (Gy^{-1} cell^{-1}) of the ith type of clustered damage. For the uniform irradiation conditions assumed in the MCDS, the absorbed dose is equal to the product of the expected number of primary charged particles of energy E passing through the target times the frequency-mean specific energy per event (ICRU 1983), i.e., $D(E) = v(E)\bar{z}_F(E)$. From the above definitions, it follows that the expected number of the ith type of cluster per primary charged particle traversal (track or hit) is

$$\sigma_i(E) \equiv \frac{\Sigma_i(E)D(E)}{v(E)} = \frac{\Sigma_i(E)\left[v(E)\bar{z}_F(E)\right]}{v(E)} = \Sigma_i(E)\bar{z}_F(E). \tag{1}$$

The spectrum-averaged number of the ith type of cluster, per primary charged particle traversal per cell, is given by

$$\sigma_i \equiv \frac{\int_0^\infty \mathrm{d}E \ \sigma_i(E)v(E)}{\int_0^\infty \mathrm{d}E \ v(E)} = \frac{1}{v}\int_0^\infty \mathrm{d}E \ \Sigma_i(E)v(E)\bar{z}_F(E). \tag{2}$$

Because the expected number of particles passing through a cell is proportional to fluence, equation (2) may also be rewritten as

$$\sigma_i = \frac{1}{\Phi}\int_0^\infty \mathrm{d}E \ \Sigma_i(E)\Phi(E)\bar{z}_F(E). \tag{3}$$

Here, Φ is the total fluence of primary charged particles and $\Phi(E)$ is the energy fluence of primary charged particles. The average yield of the ith type of cluster, per unit-absorbed dose per cell, is

$$\Sigma_i \equiv \frac{\sigma_i}{\bar{z}_F} = \frac{\int_0^\infty \mathrm{d}E \ \Sigma_i(E)\Phi(E)\bar{z}_F(E)}{\int_0^\infty \mathrm{d}E \ \Phi(E)\bar{z}_F(E)}. \tag{4}$$

For a uniformly irradiated spherical target of diameter d (μm) composed of matter at density ρ (g cm^{-3}), the frequency-mean specific energy is approximately equal to (ICRU 1983)

$$\bar{z}_F \cong 0.204\frac{\mathrm{LET}_\infty}{\rho d^2}. \tag{5}$$

Substitution of the right-hand side of equation (5) into equation (4) for $\bar{z}_F$ gives

$$\Sigma_i \cong \frac{\int_0^\infty dE \ \Sigma_i(E)\Phi(E)\mathrm{LET}_\infty(E)}{\int_0^\infty dE \ \Phi(E)\mathrm{LET}_\infty(E)}. \tag{6}$$

For electrons with energies higher than 1 keV, we used the unrestricted LET (stopping powers) from the National Institute of Standards and Technology (NIST) (Berger *et al* 2005). For electron energies below 1 keV, estimates of particle LET are based on a fit to the data reported by Emfietzoglou and Nikjoo (2007), i.e.

$$\mathrm{LET(eV\,nm^{-1})} = 4376T^{-1}\ln T - 19\,803T^{-1} + 1\,29\,622T^{-2} \tag{7}$$

where T is the electron energy in eV. Estimates of the $\Sigma_i(E)$ parameter in equation (6) for monoenergetic electrons were computed with the MCDS program[3] and assembled into a database with different types of clustered damage, including SSB and DSB. Estimates of the damage yields $\mathrm{Gy^{-1}\,cell^{-1}}$ were converted to units of $\mathrm{Gy^{-1}\,Gbp^{-1}}$ by multiplying by the 6 Gbp per cell DNA content used in the MCDS software (Semenenko and Stewart 2004, 2006).

2.4. Relative biological effectiveness (RBE)

RBE is usually defined as the ratio of a dose of a low LET reference radiation to the dose of another radiation needed to achieve the same biological effect. Because the induction of DNA damage is proportional to the absorbed dose up to at least a few hundred Gy of low and high LET radiation (Frankenberg *et al* 1999, Sutherland *et al* 2002, Rothkamm and Löbrich 2003), RBE can also be expressed as a ratio of damage yields, i.e.,

$$\mathrm{RBE} \equiv \frac{D_L}{D_H} = \frac{\Sigma_H}{\Sigma_L}. \tag{8}$$

Here, the subscripts L and H denote low and high LET radiations, respectively. All of the reported RBE values use γ-rays from ^{60}Co as the reference (low LET) radiation.

3. Results

3.1. Single-cell irradiation geometry

Figure 2 shows the secondary electron spectra produced by ^{60}Co, ^{137}Cs, 220 kVp x-rays and 29 kVp x-rays sources in the single-cell geometry. In panel (a) of figure 2, the solid black line shows total electron fluence, and the lines with the symbols show the electron fluence due to either the 1.173 MeV photon or the 1.332 MeV photon emitted by ^{60}Co. The lower energy peak includes secondary electrons from the 1.173 and 1.332 MeV photons whereas as the higher energy peak in the electron fluence is due exclusively to 1.332 MeV photons. Characteristic x-rays emitted by ^{137}Cs are associated with electron transitions in the K and L shells and produce small but distinct peaks in the fluence of secondary electrons (figure 2, panel (b). The average energy of the electrons produced by the unfiltered 130 kVp and 220 kVp x-ray beams are 7.86 keV and 12.6 keV, respectively. As illustrated in panel (c) of figure 2, the inclusion of a filter in the irradiation geometry shifts the electron energy spectrum to higher energies. The 50 μm Rh (mammography) filter is more effective at shifting the secondary electron spectrum to higher energies than the 30 μm Mo filter (figure 2, panel (d). The average energy of the Rh- and Mo-filtered 29 kVp electron energy spectra is 12.3 keV and

---

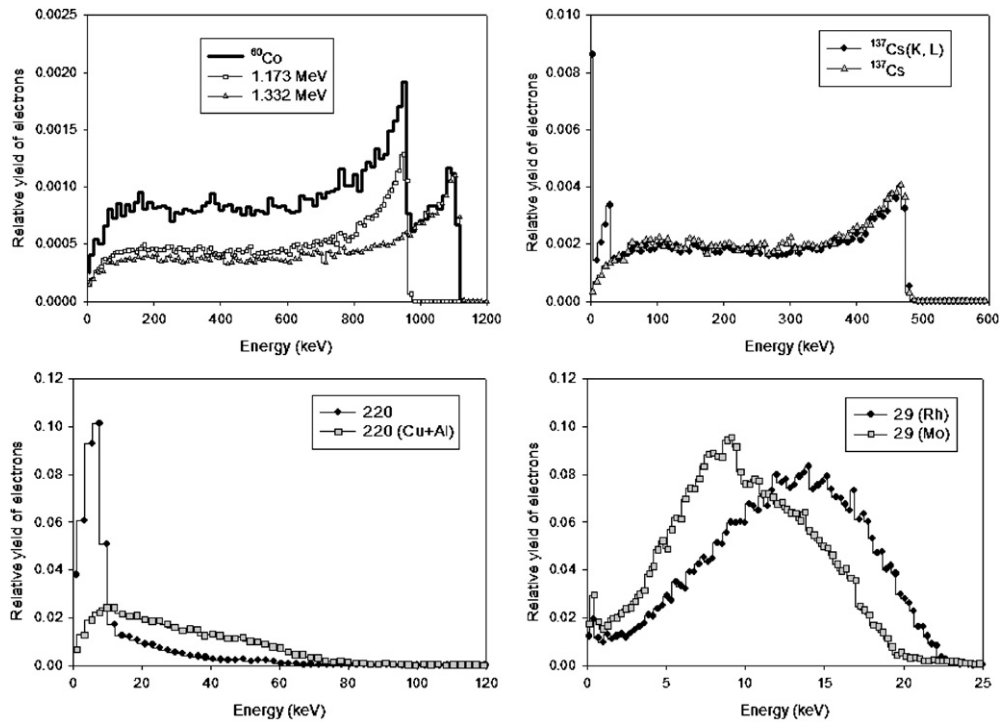[3] An executable version of the MCDS program and related information are available at http://rh.healthsciences.purdue.edu/mcds/

Figure 2. Secondary electron spectra in the single-cell geometry for selected x-ray and γ-ray sources. Panel (a) ^{60}Co; panel (b) ^{137}Cs with and without K and L-shell x-rays; panel (c) 220 kVp x-rays with and without 0.5 mm Cu and 4 mm Al filters; panel (d) 29 kVp x-rays with 50 μm Rh or 30 μm Mo filter. The (integral) area under all curves equals unity.

9.86 keV, respectively. Because electron LET increases with decreasing kinetic energy, especially below about 5 keV, the RBE for DSB induction is expected to be large for lower energy photon sources (e.g., 29 kVp x-rays) than for γ-rays from ^{60}Co or ^{137}Cs.

Table 1 compares damage yields obtained from the combined MCDS/PENELOPE simulations to results from an event-by-event (track structure) Monte Carlo code (Friedland *et al* 1999) for selected photon sources. The SSB and DSB yields estimated from the combined MCDS/PENELOPE simulations are 38% and 4% higher than those reported by Friedland *et al* (1999) for the ^{60}Co and filtered 220 kVp x-ray beams. However, the RBE for SSB and DSB induction predicted by both codes are within 1% of each other for the 220 kVp x-ray beam (by definition, the RBE is unity for ^{60}Co). This observation suggests that differences in the damage yields (Gy^{-1} Gbp^{-1}) are likely due to differences in the Monte Carlo damage simulations rather than differences in irradiation geometry or particle fluence. The RBE for DSB induction is larger than the RBE for SSB induction because DSB yields tend to increase with decreasing electron energy (increasing LET) whereas the SSB yield tends to decrease with decreasing electron energy (e.g., see figure 2 in Semenenko and Stewart 2006). The inclusion of K- and L-shell photons in the simulations for ^{137}Cs reduces the SSB by 1.6 Gy^{-1} Gbp^{-1} (<1%) and increases the DSB yield by 0.4 Gy^{-1} Gbp^{-1} (<5%). The RBE for ^{60}Co and ^{137}Cs are both very close to unity because the secondary electron spectrum is primarily composed of electrons with kinetic energies larger than 10 keV (see figure 1). For electron energies above about 10 keV, SSB and DSB damage yields are nearly constant (Semenenko and Stewart 2006).

Table 1. SSB and DSB yields for the single-cell irradiation geometry.

Energy	SSB $(Gy^{-1} Gbp^{-1})$	RBE	DSB $(Gy^{-1} Gbp^{-1})$	RBE
^{60}Co[a]	138 ± 8	1.00	8.1 ± 1.2	1.00
220 kVp				
(Cu + Al filtered)[a]	136 ± 9	0.99	8.8 ± 1.4	1.09
^{60}Co	188.3 ± 0.1	1.00	8.4 ± 0.1	1.00
^{137}Cs	188.3 ± 0.1	1.00	8.4 ± 0.1	1.00
^{137}Cs (with K,L)	186.7 ± 0.1	0.99	8.8 ± 0.1	1.05
220 kVp (unfiltered)	181.7 ± 0.1	0.97	10.1 ± 0.1	1.20
220 kVp				
(Cu + Al filtered)	186.7 ± 0.1	0.99	9.1 ± 0.1	1.08
130 kVp (unfiltered)	178.3 ± 0.1	0.95	10.9 ± 0.1	1.30
130 kVp (Cu filter)	185.0 ± 0.1	0.98	9.4 ± 0.1	1.12
29 kVp (Rh filter)	183.3 ± 0.1	0.97	9.8 ± 0.1	1.16
29 kVp (Mo filter)	181.7 ± 0.1	0.97	10.0 ± 0.1	1.19

[a] As reported by Friedland et al (1999).

To further study the contribution to the DSB yield of electrons below 10 keV, we investigated the impact of different radiation transport parameters and fluence-binning strategies. The DSB yields for the filtered 220 kVp x-ray beam increased from 9.1 Gy^{-1} Gbp^{-1} (table 1) for 100 energy-fluence bins to 9.2 Gy^{-1} Gbp^{-1} for 200 energy-fluence bins (2% increase). The DSB yield for 220 kVp x-rays decrease by less than 2% when PENELOPE transport parameters are changed from $C_1 = 0.00$, $C_2 = 0.01$, $W_{CC} = 100$ eV, $W_{CR} = 100$ eV to $C_1 = 0.2$, $C_2 = 0.1$, $W_{CC} = 1$ keV, $W_{CR} = 1$ keV, which suggests that the details of the very low-energy electron transport have a nominal impact on estimates of the overall yield of DSB.

3.2. Monolayer cell culture irradiation geometry

Table 2 compares the MCDS/PENELOPE damage yields for the monolayer cell culture geometry to published experimental results. The measured DSB yields for the ^{60}Co and 29 kVp x-ray beam with Rh filter reported by Kühne et al (2005) are about 40% lower than the corresponding DSB yields predicted from the MCDS/PENELOPE simulation. However, the measured and predicted RBE for 29 kVp x-ray beam is nearly the same (1.15 versus 1.16). The differences in measured and predicted DSB yields may be attributed to the loss of small fragments in the pulsed-field gel electrophoresis (PFGE) assay (Rydberg et al 2002, Friedland et al 2005, Semenenko and Stewart 2006).

Table 3 lists damage yields for several radioisotopes commonly used in laboratory experiments and brachytherapy. The damage yields reported in table 3 are based on particle fluences in the monolayer cell culture geometry. The predicted DSB yields for the isotopes listed in table 3 differ by at most 16% (i.e. from 8.4 Gy^{-1} Gbp^{-1} to 9.7 Gy^{-1} Gbp^{-1}) and the SSB yields differ by less than 3%. Damage yields for ^{60}Co and ^{192}Ir are the same within the precision of the calculations because these isotopes primarily emit higher energy photons, and differences in the RBE of photon sources are due to electrons with energies less than about 10 keV. The effect of the 50 μm titanium shell has less than a 1% effect on the SSB and DSB yields for all studied isotopes. The RBE of ^{169}Yb, 1.06, is close to the RBE for cell survival of 1.2 ± 0.3 reported by Plume et al (1993). The predicted RBE for DSB induction of 1.16 for

Table 2. SSB and DSB yields for the cell culture geometry.

Energy	SSB Gy^{-1} Gbp^{-1}	SSB RBE	DSB Gy^{-1} Gbp^{-1}	DSB RBE
Co[a]	N/A	N/A	6.1 ± 0.2	1.00
29 kVp (Rh filter)[a]	N/A	N/A	7.0 ± 0.2	1.15
Co	189.2 ± 0.1	1.00	8.4 ± 0.1	1.00
Cs137 (with K,L)	188.3 ± 0.1	1.00	8.4 ± 0.1	1.00
220 kVp (unfiltered)	185.0 ± 0.1	0.98	9.3 ± 0.1	1.11
220 kVp (Cu + Al filtered)	186.7 ± 0.1	0.99	9.1 ± 0.1	1.08
130 kVp (unfiltered)	185.0 ± 0.1	0.98	9.5 ± 0.1	1.13
130 kVp (Cu filter)	185.0 ± 0.1	0.98	9.3 ± 0.1	1.11
29 kVp (Rh filter)	183.3 ± 0.1	0.97	9.7 ± 0.1	1.16
29 kVp (Mo filter)	183.3 ± 0.1	0.97	9.8 ± 0.1	1.17

[a] Experimental results reported by Kühne *et al* (2005).

Table 3. SSB and DSB yields for selected isotopes (used in laboratory experiments and brachytherapy).

Source	SSB (Gy^{-1} Gbp^{-1})	SSB RBE	DSB (Gy^{-1} Gbp^{-1})	DSB RBE
^{60}Co	189.2 ± 0.1	1.00	8.4 ± 0.1	1.00
^{192}Ir	188.3 ± 0.1	1.00	8.4 ± 0.1	1.00
^{169}Yb	186.7 ± 0.1	0.99	8.9 ± 0.1	1.06
^{131}Cs	183.3 ± 0.1	0.97	9.6 ± 0.1	1.14
^{125}I	183.3 ± 0.1	0.97	9.7 ± 0.1	1.16

^{125}I is also quite similar to published (Hering 1980, Freeman *et al* 1982, Marchese *et al* 1984, Ling *et al* 1995, Lehnert *et al* 2005) RBE values (1.2–1.5) derived from cell survival data.

4. Summary and discussion

The results shown in tables 1 and 2 indicate that the DSB for the single-cell and monolayer cell culture geometry differ by at most 15%. The differences in the DSB yields are most pronounced for the unfiltered 130 kVp x-ray beam (RBE of 1.30 and 1.13 for the single-cell and cell culture geometries, respectively). For the filtered 130 and 220 kVp x-ray beams and the 29 kVp filtered x-rays, RBE values for DSB induction differ by less than 3%. For the filtered and unfiltered x-ray beams, the RBE values for SSB induction are differ by at most 5% (unfiltered 130 kVp x-ray beam) for the single-cell and monolayer cell culture geometry. For photon sources that are primary composed of high-energy photons (e.g. ^{60}Co) or low-energy photons (29 kVp filtered x-rays), the choice of a single-cell or monolayer cell culture geometry has a nominal impact on the predicted RBE values. However, photon sources that produce a mixture of low- and high-energy photons are potentially sensitive to the choice of geometry. For example, the inclusion of secondary electrons associated with the emission of K- and L-shell characteristic x-rays increases the RBE of ^{137}Cs for the single-cell geometry (table 1) by 5% whereas the inclusion of K- and L-shell x-rays has a negligible ($< 0.5\%$) impact on the RBE for monolayer cell cultures (table 2).

The RBE for SSB induction ranges from 0.95 to 0.98 for typical diagnostic x-ray sources. However, the RBE for DSB induction is substantially larger than unity even for the 220 kVp

filtered x-ray source. For 220 kVp x-rays, the predicted RBE for DSB induction ranges from 1.08 (filtered) to 1.20 (unfiltered). The RBEs for the 130 kVp x-ray beams are even larger (1.12 for the filtered and 1.30 for the unfiltered). The predicted RBEs for DSB induction by the 29 kVp Rh- and Mo-filtered x-rays beams used in mammography are 1.16 and 1.19, respectively. These observations suggest that the x-ray beams used for diagnostic purposes are biologically more effective than γ-rays from ^{137}Cs or ^{60}Co.

The RBE for DSB induction by ^{169}Yb, ^{131}Cs and ^{125}I in the monolayer cell culture geometry ranges from 1.06 to 1.16 and from 1.17 to 1.39 for the single-cell geometry. The RBE for SSB varies by at most 7% among these isotopes. If a 50 μm titanium shell is added, the RBE range decreases to 1.05–1.20 (up to 16% reduced). In contrast to the single-cell geometry, the titanium encapsulation has a negligible impact on the SSB and DSB yields in the monolayer cell culture geometry because the low-energy electrons are absorbed in either the 5 mm layer of water (culture medium) or 50 μm titanium shell. When taken together, these observations suggest that the RBEs for DSB induction by encapsulated brachytherapy sources are nearly the same for the single-cell and monolayer cell culture geometries.

We found that the RBE for DSB induction by 29 kVp x-rays relative to 220 kVp x-rays is at most 1.10 (RBE result for the 30 μm Mo filter). In contrast, Frankenberg *et al* (2002) report that the limiting RBE (ratio of α in the linear-quadratic cell survival model) for the human hybrid (Hela × normal human skin fibroblasts) CGL1 cell line irradiated by 29 kVp x-rays relative to 200 kVp x-rays is 4.38 ± 1.87. They also found that the RBE for neoplastic transformation is 4.3 for doses less than or equal to 0.5 Gy and 1.9 for 4 Gy (Frankenberg *et al* 2002). Heyes and Mill (2004) report that the RBE for neoplastic transformation of CGL1 cells by 29 kVp x-rays relative to β^- radiation from ^{90}Sr/^{90}Y is 5.16 ± 3.50. The poor agreement among the predicted RBE for DSB induction by low-energy photons and the experimental RBE values suggests that biophysical processes other than DSB induction, such as bystander effects (Seymour and Mothersill 2000, Schettino *et al* 2003, 2005) and damage repair, contribute substantially to the RBE of low-energy photons for the endpoints of clonogenic cell survival and neoplastic transformation.

For very low-energy photons, secondary electrons are mainly produced through photoelectric absorption. The photoelectrons produced in these interactions are nearly monoenergetic, and the MCDS can be used to directly estimate damage yields without the need for PENELOPE simulations. For V79 cells irradiated by K-shell (280 eV) characteristic x-rays, de Lara *et al* (2001) report a DSB yield of 20.7 Gy^{-1} Gbp^{-1}. For comparison, the MCDS predicts a DSB yield of 20.7 Gy^{-1} Gbp^{-1} for electrons with a kinetic energy of 238 eV (= 280 eV minus 42 eV for the binding energy of electrons in the L$_I$ shell of oxygen, Cardona and Ley (1978)). For the irradiation of V79 cells by aluminum K-shell (1.49 keV) characteristic x-rays, Botchway *et al* (1997) report a DSB yield of 14.3 Gy^{-1} Gbp^{-1} compared to the MCDS-predicted yield of 13.4 Gy^{-1} Gbp^{-1} for 947 eV electrons (=1490 eV–543 eV for binding energy of electrons in the K shell of oxygen, Cardona and Ley (1978)). The close agreement among the measured and predicted DSB yields ($\leqslant$7% difference) suggests that the MCDS is capable of accurately predicting DSB yields in V79 cells irradiated by very low-energy photons.

We have shown that the proposed algorithm for estimating the RBE for diagnostic and characteristic x-rays and selected low-energy γ-ray-emitting radioisotopes are comparable to measured damage yields (table 2) and to the results of selected track structure simulations (table 1). However, equation (6) is equally applicable to other types of charged particles, and RBE values for the induction of damage by mixtures of protons and/or α particles could be computed using a similar approach. A major advantage of the proposed methodology is that damage yields for the passage of monoenergetic charged particles through single cells can

be assembled into a database and then used to predict spectrum-averaged damage yields for other irradiation geometries in a computationally efficient manner. Such a methodology may be particularly useful for applications that involve radiation transport through materials other than water or for applications that are too computationally intensive for event-by-event (track structure) Monte Carlo methods, such as computing the biological effectiveness of proton therapy treatments or complex distributions of low- and high-LET radioisotopes inside the human body.

Acknowledgment

References

Baró J, Sempau J, Fernández-Varea J M and Salvat F 1995 PENELOPE: an algorithm for Monte Carlo simulation of the penetration and energy loss of electrons and positrons in matter *Nucl. Instrum. Methods Phys. Res.* B **100** 31–46

Belli M, Cherubini R, Dalla Vecchia M, Dini V, Moschini G, Signoretti C, Simone G, Tabocchini M A and Tiveron P 2000 DNA DSB induction and rejoining in V79 cells irradiated with light ions: a constant field gel electrophoresis study *Int. J. Radiat. Biol.* **76** 1095–104

Berger M J, Coursey J S, Zucker M A and Chang J 2005 Stopping-power and range tables for electrons, protons, and helium ions ESTAR program National Institute of Standards and Technology http://physics.nist.gov/PhysRefData/Star/Text/contents.html (last updated August 2005; accessed on Jan 24, 2007)

Botchway S W, Stevens D L, Hill M A, Jenner T J and O'Neill P 1997 Induction and rejoining of DNA double-strand breaks in Chinese hamster V79–4 cells irradiated with characteristic aluminum K and copper L ultrasoft X rays *Radiat. Res.* **148** 317–24

Cardona M and Ley L 1978 *Photoemission in Solids: General Principles* (Berlin: Springer)

Chen Z, Bongiorni P and Nath R 2005 Dose rate constant of a Cesium-131 interstitial brachytherapy seed measured by thermoluminescent dosimetry and gamma-ray spectrometry *Med. Phys.* **32** 3279–85

Claesson A K, Stenerlöw B, Jacobsson L and Elmroth K 2007 Relative biological effectiveness of the α-particle emitter [211]At for double-strand break induction in human fibroblasts *Radiat. Res.* **167** 312–8

de Lara C M, Hill M A, Jenner T J, Papworth D and O'Neill P 2001 Dependence of the yield of DNA double-strand breaks in Chinese hamster V79–4 cells on the photon energy of ultrasoft X rays *Radiat. Res.* **155** 440–8

Emfietzoglou D and Nikjoo H 2007 Accurate electron inelastic cross sections and stopping powers for liquid water over the 0.1–10 keV range based on an improved dielectric description of the Bethe surface *Radiat. Res.* **167** 110–20

Frankenberg D, Brede H J, Schrewe U J, Steinmetz C, Frankenberg-Schwager M, Kasten G and Pralle E 1999 Induction of DNA double-strand breaks by ^{1}H and [4]He ions in primary human skin fibroblasts in the LET range of 8 to 124 keV/μm *Radiat. Res.* **151** 540–9

Frankenberg D, Kelnhofer K, Bär K and Frankenberg-Schwager M 2002 Enhanced neoplastic transformation by mammography X rays relative to 200 kVp X rays: indication for a strong dependence on photon energy of the RBE_M for various end points *Radiat. Res.* **157** 99–105

Freeman M L, Goldhagen P, Sierra E and Hall E J 1982 Studies with encapsulated 125I sources: II. Determination of the relative biological effectiveness using cultured mammalian cells *Int. J. Radiat. Oncol. Biol. Phys.* **8** 1355–61

Friedland W, Dingfelder M, Jacob P and Paretzke H G 2005 Calculated DNA double-strand break and fragmentation yields after irradiation with He ions *Radiat. Phys. Chem.* **72** 279–86

Friedland W, Jacob P, Paretzke H G, Merzagora M and Ottolenghi A 1999 Simulation of DNA fragment distributions after irradiation with photons *Radiat. Environ. Biophys.* **38** 39–47

Goodhead D T 1994 Initial events in the cellular effects of ionizing radiations: clustered damage in DNA *Int. J. Radiat. Biol.* **65** 7–17

Hall E J 2000 *Radiobiology for the Radiologist* (Philadelphia, PA: Lippincott Williams & Wilkins)

Hering E R 1980 A comparison of the biological effect of ^{125}I and ^{192}Ir gamma rays on the roots of Vicia faba using a specially designed applicator *Br. J. Radiol.* **53** 255–8

Heyes G J and Mill A J 2004 The neoplastic transformation potential of mammography x rays and atomic bomb spectrum radiation *Radiat. Res.* **162** 120–7

ICRU 1983 *Microdosimetry Report* 36 *(Bethesda, MD: International Commission on Radiation Units and Measurements)*

Kellerer A M 2002 Electron spectra and the RBE of x rays *Radiat. Res.* **158** 13–22

Kühne M, Urban G, Frankenberg D and Löbrich M 2005 DNA double-strand break misrejoining after exposure of primary human fibroblasts to CK characteristic X rays, 29 kVp X rays and 60Co gamma rays *Radiat. Res.* **164** 669–76

Kundrát P and Stewart R D 2006 On the biophysical interpretation of lethal DNA lesions induced by ionizing radiation *Radiat. Prot. Dosim.* **122** 169–72

Lehnert S, Reniers B and Verhaegen F 2005 Relative biologic effectiveness in terms of tumor response of 125I implants compared with 60Co gamma rays *Int. J. Radiat. Oncol. Biol. Phys.* **63** 224–9

Ling C C, Li W X and Anderson L L 1995 The relative biological effectiveness of I-125 and Pd-103 *Int. J. Radiat. Oncol. Biol. Phys.* **32** 373–8

Marchese M J, Hall E J and Hilaris B S 1984 Encapsulated iodine-125 in radiation oncology: I. Study of the relative biological effectiveness (RBE) using low dose rate irradiation of mammalian cell cultures *Am. J. Clin. Oncol.* **7** 607–11

Nikjoo H and Goodhead D T 1991 Track structure analysis illustrating the prominent role of low-energy electrons in radiobiological effects of low-LET radiations *Phys. Med. Biol.* **36** 229–38

Ottolenghi A, Merzagora M and Paretzke H G 1997 DNA complex lesions induced by protons and α-particles: track structure characteristics determining linear energy transfer and particle type dependence *Radiat. Environ. Biophys.* **36** 97–103

Plume C A, Daly S E, Porter A T, Barnett R B and Battista J J 1993 The relative biological effectiveness of ytterbium-169 for low dose rate irradiation of cultured mammalian cells *Int. J. Radiat. Oncol. Biol. Phys.* **25** 835–40

Rivard M J 2007 Brachytherapy dosimetry parameters calculated for a ^{131}Cs source *Med. Phys.* **34** 754–62

Rothkamm K and Löbrich M 2003 Evidence for a lack of DNA double-strand break repair in human cells exposed to very low x-ray doses *Proc. Natl. Acad. Sci. USA.* **100** 5057–62

Rydberg B, Heilbronn L, Holley W R, Löbrich M, Zeitlin C, Chatterjee A and Cooper P K 2002 Spatial distribution and yield of DNA double-strand breaks induced by 3–7 MeV helium ions in human fibroblasts *Radiat. Res.* **158** 32–42

Säbel M and Aichinger H 1996 Recent developments in breast imaging *Phys. Med. Biol.* **41** 315–68

Salvat F, Fernandez-Varea J M and Sempau J 2003 PENELOPE—a code system for Monte Carlo simulation of electron and photon transport

Salvat F, Fernandez-Varea J M and Sempau J 2005 PENELOPE

Schettino G, Folkard M, Michael B D and Prise K M 2005 Low-dose binary behavior of bystander cell killing after microbeam irradiation of a single cell with focused C_K x rays *Radiat. Res.* **163** 332–6

Schettino G, Folkard M, Prise K M, Vojnovic B, Held K D and Michael B D 2003 Low-dose studies of bystander cell killing with targeted soft x rays *Radiat. Res.* **160** 505–11

Semenenko V A and Stewart R D 2004 A fast Monte Carlo algorithm to simulate the spectrum of DNA damages formed by ionizing radiation *Radiat. Res.* **161** 451–7

Semenenko V A and Stewart R D 2006 Fast Monte Carlo simulation of DNA damage formed by electrons and light ions *Phys. Med. Biol.* **51** 1693–706

Sempau J, Acosta E, Baró J, Fernández-Varea J M and Salvat F 1997 An algorithm for Monte Carlo simulation of coupled electron-photon transport *Nucl. Instrum. Methods Phys. Res.* B **132** 377–90

Seymour C B and Mothersill C 2000 Relative contribution of bystander and targeted cell killing to the low-dose region of the radiation dose-response curve *Radiat. Res.* **153** 508–11

Spadinger I and Palcic B 1992 The relative biological effectiveness of ^{60}Co gamma-rays, 55 kVp X-rays, 250 kVp X-rays, and 11 MeV electrons at low doses *Int. J. Radiat. Biol.* **61** 345–53

Stewart R D, Wilson W E, McDonald J C and Strom D J 2002 Microdosimetric properties of ionizing electrons in water: a test of the PENELOPE code system *Phys. Med. Biol.* **47** 79–88

Sutherland B M, Bennett P V, Sutherland J C and Laval J 2002 Clustered DNA damages induced by x rays in human cells *Radiat. Res.* **157** 611–6

Verhaegen F and Reniers B 2004 Microdosimetric analysis of various mammography spectra: lineal energy distributions and ionization cluster analysis *Radiat. Res.* **162** 592–9

Walicka M A, Adelstein S J and Kassis A I 1998 Indirect mechanism contribute to biological effects produced by decay of DNA-incorporated iodine-125 in mammalian cells *in vitro*: double strand breaks *Radiat. Res.* **149** 134–41

Ward J F 1988 DNA damage produced by ionizing radiation in mammalian cells: identities, mechanisms of formation, and reparability *Prog. Nucl. Acid. Res. Mol. Biol.* **35** 95–125